ARTICLE



Super resolution NOESY spectra of proteins

Charles F. DeLisle¹ · H. Bhagya Mendis¹ · Justin L. Lorieau¹

Received: 30 October 2018 / Accepted: 30 January 2019 / Published online: 30 April 2019 © Springer Nature B.V. 2019

Abstract

Spectral resolution remains one of the most significant limitations in the NMR study of biomolecules. We present the srNOESY (super resolution nuclear overhauser effect spectroscopy) experiment, which enhances the resolution of NOESY cross-peaks at the expense of the diagonal peak line-width. We studied two proteins, ubiquitin and the influenza hemagglutinin fusion peptide in bicelles, and we achieved average resolution enhancements of 21–47% and individual peak enhancements as large as ca. 450%. New peaks were observed over the conventional NOESY experiment in both proteins as a result of these improvements, and the final structures generated from the calculated restraints matched published models. We discuss the impact of the experimental parameters, spin diffusion and the information content of the srNOESY lineshape.

Keywords Solution-state NMR · NOESY · Resolution enhancement · Proteins · Signal improvement · SRNOESY

Introduction

NMR spectroscopy is a valuable tool in the elucidation of bonding topology, molecular structure and molecular dynamics in chemistry and structural biology. Yet, the complexity and size of interesting biomolecules still limits the utility of NMR in structural studies. As molecules become larger, the number of resonances grows with the number of atoms and tumbling (rotational) times increase, thereby producing lower resolution spectra with broadened and more numerous peaks. Consequently, the study of large biomolecules is prohibitive by NMR. Different approaches mitigate these problems, including methyl spectroscopy (Ollerenshaw et al. 2003; Tugarinov and Kay 2005; Chi et al. 2018; Otten et al. 2010), transverse relaxation optimized spectroscopy (Pervushin et al. 1997; Weigelt 1998), partial deuteration and site-specific labeling (LeMaster and Richards 1988; Ellman et al. 1992; Battiste and Wagner 2000), and resolution enhancement with constant-time evolution (Vuister and Bax 1992). These approaches often require specialized

Electronic supplementary material The online version of this article (https://doi.org/10.1007/s10858-019-00231-x) contains supplementary material, which is available to authorized users.

samples to study only a subset of atoms in a molecule, and may require a priori knowledge of the molecular structure. Importantly, they may preclude essential structural information, such as the distance restraints of perdeuterated molecules collected through NOESY spectra (Vögeli et al. 2010; Rieping et al. 2007), which benefits from extensive ¹H spin labeling.

In this article, we present an easily implemented approach to the resolution enhancement of fully protonated molecules with NOESY spectroscopy. We achieve average linewidth reductions of 16–32% (resolution enhancements of 21–47%) and linewidth reductions as large as 78% to resolve new cross-peaks not observed in conventional NOESY experiments. These enhancements represent apparent linewidths that are narrower than the natural linewidth for a given resonance.

Our approach uses a time-dependent NOE mix period (t_{mix}) that increments with the evolution period in the indirect ¹H dimension, t_I . A NOESY experiment with a linear time-dependent mixing time was previously reported for the suppression of J-couplings in spectra (Macura et al. 1982a, b). However, the aim of those studies was to minimally change the NOE mix time (ca. 20% of t_{mix}) to maintain a relatively constant NOE cross-peak intensity while suppressing coherent J-coupling transfers. Our approach incorporates significant changes in the NOE mix time (ca. 300–500% of t_{mix}) to utilize the signal buildup of a cross-peak to enhance its resolution.



[✓] Justin L. Lorieau justin@lorieau.com

Department of Chemistry, University of Illinois at Chicago, 845 West Taylor Street, Chicago, IL 60607, USA

The srNOESY uses two concepts to improve the quality of spectra. At short t_1 values in the indirect dimension, the t_{mix} is small and close to its initial value. The intensity of a peak is emphasized in the initial evolution of a time-dependent signal, and the resolution is emphasized in the later portions. Shorter t_{mix} periods are desirable for accurate NOESY distance restraints because spin diffusion pathways are minimally expressed in this regime (Borgias et al. 1990; Baleja et al. 1990). Second, at longer t_1 values, the t_{mix} is significantly increased from its initial value to utilize the signal buildup of the cross-peak to enhance resolution. At longer t_{mix} periods, direct transfer and spin diffusion pathways continue to transfer magnetization between spins to increase the intensity of crosspeaks, yet this additional intensity is typically discarded in favor of greater accuracy for NOE distance restraints. The srNOESY experiment utilizes this buildup period to enhance the resolution of cross-peaks while having a minimal impact on the accuracy of cross-peak intensities.

Materials and methods

Sample preparation

A DNA sequence for ubiquitin was subcloned in pET-15b (Genscript), and the plasmid was transformed into Escherichia coli BL21(DE3) cells (Fisher). Expression of uniformly ¹⁵N-labeled ubiquitin was achieved as previously described (Marley et al. 2001). Bacterial cells were lysed by sonication in a pH 7.8 buffer containing 50 mM Tris, 500 mM NaCl and 20 mM imidazole. The resulting slurry was centrifuged at 70,000 x g for 30 min at 4 °C. The protein solution was passed through a His-Trap column (GE) with an AKTA Start FPLC (GE) and eluted with the lysis buffer containing an additional 250 mM imidazole. The purity of the sample was confirmed by SDS-PAGE. The folded structure of a 0.8 mM ¹⁵N-labeled ubiquitin sample in 10 mM sodium phosphate, 0.03% NaN₃ and 7% D₂O at pH 6.6 and 25 °C was confirmed with an ¹⁵N-HSQC spectrum compared to published chemical shifts (Cornilescu et al. 1998).

Influenza HAfp expression and purification was achieved as previously described (Lorieau et al. 2010; Smrt et al. 2015), with a final size-exclusion chromatography step using a Superdex 75 26/600 PG column (GE). The sample purity was confirmed with SDS-PAGE and MALDI-TOF mass spectrometry. The folded structure of 1.0 mM $^{15}\text{N-labeled}$ HAfp in 30 mM Tris-d₁₁ with q=0.44 bicelles with 44 mM $^2\text{H-dimyristoylphosphatidylcholine}$ ($^2\text{H-DMPC}$) and 100 mM dihexanoylphosphatidylcholine (DHPC), 0.03% NaN₃, 10% D₂O at pH 7.2 was confirmed with published $^{15}\text{N-HSQC}$ chemical shifts (Lorieau et al. 2010).



NMR spectra were recorded for uniformly ¹⁵N-labeled ubiquitin (10 mM sodium phosphate, 93% H₂O/7% D₂O at pH 6.6 and a temperature of 25 °C) and uniformly 15 N-labeled HAfp bound to q = 0.44 2 H-DMPC/DHPC bicelles (30 mM Tris-d₁₁, 44 mM DMPC-d₅₄, 100 mM DHPC, 90% H₂O/10% D₂O at pH 7.2 and a temperature of 32 °C). A Bruker AVIII-750 wide-bore spectrometer equipped with a ¹H/¹³C/¹⁵N TXI 5 mm room temperature probe was used for all NOESY-HSQC and HAfp-bicelle ¹⁵N relaxation experiments. A Bruker AVIII-500 widebore spectrometer equipped with a ¹H/¹³C/¹⁵N TXI 5 mm room temperature probe was used for ubiquitin ¹⁵N relaxation experiments. Spectra were apodized using a sine-bell function with an initial value of 0.45π and a final value of 0.90π , and processed with zero-filling to 1024 points in the indirect ¹H dimension, 512 points in the ¹⁵N indirect dimension, and 2048 points in the direct ¹H dimension.

Data analysis

NMRPipe (Delaglio et al. 1995) was used to process all NMR data, and Sparky (Lee et al. 2015; Goddard and Kneller 2008) was selected for NOESY peak shape analysis due to its peak deconvolution features. The correlation times of each system were determined by fitting the ¹⁵N relaxation rates using FAST-Modelfree within the NMR-box software suite (Lipari and Szabo 1982a, b; Cole et al. 2003; Maciejewski et al. 2017). The ¹⁵N R₁, R_{1ρ}, R₂, and {¹H}-¹⁵N NOE rates were determined for both systems as previously described (Smrt et al. 2015).

A structure refinement using Xplor-NIH (Schwieters and Kuszewski 2006) v2.47 with simulated annealing was performed with the inclusion of published NOESY distance restraints replaced with data from the srNOESY-HSQC spectra in this study. The simulations matched the published protocols for the structures. Data for ubiquitin were obtained from PDB ID 1D3Z¹⁸ and data for HAfp were obtained from 2KXA¹⁹.

Theory

Cross-relaxation in a homonuclear [¹H,¹H]-NOESY experiment is governed by large relaxation matrices that couple the direct transfer of magnetization between two spins as well as numerous indirect spin diffusion pathways through local and intermediary spins (Borgias et al. 1990). In the simplest case, the direct cross-relaxation between two spins, 'i' and 's,' is represented by two coupled different



equations and a 2×2 relaxation matrix (Borgias et al. 1990; Dobson et al. 1982; Vögeli et al. 2009):

$$\begin{split} \frac{d\Delta I_z(t)}{dt} &= -R_{1,i}\Delta I_z(t) - \sigma_{is}\Delta S_z(t) \\ \frac{d\Delta S_z(t)}{dt} &= -\sigma_{is}\Delta I_z(t) - R_{1,s}\Delta S_z(t) \end{split} \tag{1}$$

 $\Delta I_z(t)$ is the deviation from the Boltzmann equilibrium magnetization for the diagonal peak and $\Delta S_z(t)$ is the magnetization for the cross-peak. $R_{1,i}$ and $R_{1,s}$ are the autorelaxation rates for spins 'i' and 's', and σ_{is} is the cross-relaxation (NOE) rate between spins 'i' and 's.' These can be calculated using semi-classical theory and spectral density functions ($J(\omega)$) at spectrometer frequencies ' ω ' (Dobson et al. 1982; Farrow et al. 1994):

$$R_{1,i} = \frac{\gamma_H^4 \hbar^2}{10} \sum_{\substack{s=1\\s \neq i}}^{spins} \frac{1}{\left\langle r_{is}^6 \right\rangle} \left(1J(0) + 3J(\omega_H) + 6J(2\omega_H) \right)$$

$$\sigma_{is} = \frac{\gamma_H^4 \hbar^2}{10} \frac{1}{\left\langle r_{is}^6 \right\rangle} \left(6J(2\omega_H) - 1J(0) \right)$$
(2)

The gyromagnetic ratio of ${}^{1}H$ is represented by γ_{H} and \hbar is the Planck constant. The $\langle r_{is}^{6} \rangle$ term is the internuclear distance to the 6th power for spins 'i' and 's.' The angle brackets denotes a motionally averaged value over r_{is}^{6} from internal motions on a picosecond timescale.

For simplicity, we have neglected the contribution of the ^{1}H chemical shift anisotropy since the ^{1}H – ^{1}H dipolar interaction dominates ^{1}H relaxation at the NMR fields measured (500- and 750-MHz). The spectral density function, $J(n\omega)$, may adopt a variety of functional forms depending on the type and timescale of internal and overall motions for a molecule (Lipari and Szabo 1982a, b). The simplest form is represented by a molecule in solution that is internally rigid and that tumbles (rotates) isotropically with a correlation time τ_c , where n represents the zero, single, or double quantum transitions.

$$J(n\omega) = \frac{\tau_c}{1 + (n\omega\tau_c)^2} \tag{3}$$

In a 750-MHz NMR spectrometer, the zero-quantum J(0) term dominates the auto- and cross-relaxation rates when the τ_c is above 0.3 ns, representing internally-rigid molecules larger than approximately 700 Daltons (Schimmel 1980). This condition is known as the 'spin-diffusion' regime, and it will be used in the analysis of the large, folded biomolecules in this study. The general principles of the srNOESY are nevertheless applicable to smaller molecules.

In the spin-diffusion limit, the auto- and cross-relaxation rates can be simplified.

$$\sigma_{is} = -\frac{\gamma_H^4 \hbar^2}{10} \tau_c \frac{1}{\left\langle r_{is}^6 \right\rangle}$$

$$R_{1,i} = \frac{\gamma_H^4 \hbar^2}{10} \tau_c \sum_{\substack{s=1\\s \neq i}}^{spins} \frac{1}{\left\langle r_{is}^6 \right\rangle} = -\sum_{\substack{s=1\\s \neq i}}^{spins} \sigma_{is}$$
(4)

For a large molecule with no internal motion, σ_{is} is negative and the R_1 rates are positive. These rates represent the maximum magnitudes for the rates at a given τ_c , and fast internal motions will reduce their magnitude. Additionally, the $R_{2,i}$ rate, or rate of transverse relaxation of 1H spin 'i', is evaluated as follows (Farrow et al. 1994):

$$R_{2,i} = \frac{\gamma_H^4 \hbar^2}{20} \sum_{\substack{s=1\\s \neq i}}^{spins} \frac{1}{\left\langle r_{is}^6 \right\rangle} \left(9J(\omega_H) + 5J(0) + 6J(2\omega_H) \right)$$

$$= -\frac{5}{2} \sum_{\substack{s=1\\s \neq i}}^{spins} \sigma_{is}$$
(5)

The R_2 rates are also positive.

In two-dimensional NOESY experiments, or NOESY experiments with higher dimensionalities, the contribution of cross-relaxation and auto-relaxation can be resolved from cross-peaks, $\Delta S_z(t)$, and diagonal peaks, $\Delta I_z(t)$, respectively. The coupled differential Eq. (1) can be solved analytically (Vögeli et al. 2009). For simplicity, we present a solution for the buildup of the cross-peak magnetization, $\Delta S_z(t)$, when the auto-relaxation rates, $R_{1,i}$ and $R_{1,s}$, are approximately equal ($R_{1,i} = R_{1,s} = R_1$):

$$\Delta I_z(t) = \cosh(\sigma_{is}t) \cdot \exp(-R_1t) \cdot \Delta I_z(0)$$

$$\Delta S_z(t) = \sinh(\sigma_{is}t) \cdot \exp(-R_1t) \cdot \Delta I_z(0)$$
(6)

Note that our derivation of Eq. (2) from Vögeli et al. (2009) reads as follows:

$$\frac{\Delta I_z(t)}{\Delta I_z(0)} = \frac{1}{2} \left[\left(1 + \frac{\rho_I - \rho_S}{\lambda_+ - \lambda_-} \right) e^{-\lambda_- t} + \left(1 - \frac{\rho_I - \rho_S}{\lambda_+ - \lambda_-} \right) e^{-\lambda_+ t} \right]$$
(7)

Initially, the system has an initial magnetization for the donor spin ($\Delta I_z(0) \neq 0$) and the cross-peak magnetization is zero ($\Delta S_z(0) = 0$). In the limit that the auto-relaxation rate is small or the mix time is short (i.e. $R_1 t \approx 0$), the cross-peak follows a linear buildup, as previously described (Baleja et al. 1990). At long mixing times, the cross-peak and diagonal peak magnetizations reach their Boltzmann equilibrium values due to the exponential decay, $\exp(-R_1 t)$.



For a two-dimensional, or higher dimensional NOESY experiment, the initial magnetization is modulated by the chemical shift (ω_{CS}) and $^{1}\text{H R}_{2}$ relaxation in the evolution period prior to the NOE mixing block.

$$Re\{\Delta S_z(t_{mix}, t_1)\} = \cos(\omega_{CS}t_1) \cdot \exp(-R_2t_1) \cdot \Delta S_z(t_{mix})$$

$$Im\{\Delta S_z(t_{mix}, t_1)\} = \sin(\omega_{CS}t_1) \cdot \exp(-R_2t_1) \cdot \Delta S_z(t_{mix})$$
(8)

With TPPI or States acquisition modes, the real and imaginary components are collected by incrementing the phase of the first or second NOESY pulse by 90°.

To simplify the analytic expression, Eq. (6) can be expressed in the linear build-up regime for the cross-peak $(\Delta S(t))$ using a Taylor expansion for the $\sinh(\sigma_{is}t)$ function.

$$\Delta S(t) = \sigma_{is}t \cdot \exp(-R_1 t) \tag{13}$$

This function has the same initial time dependence as the cross-peak function in Eq. (6), yet the function decays more quickly at longer mixing times. Consequently, the predicted srNOESY resolution enhancement will be smaller than the experimental enhancement, using this approximation.

We then evaluate the behavior of the cross-peak in the srNOESY.

$$\operatorname{Re}\{I_{ij}(t_{1})\} = \cos(\omega_{CS}t_{1}) \cdot \sigma_{ij}(a_{0} + a_{1}t_{1}) \cdot \exp(-R_{2,i}t_{1} - R_{1}a_{0} - R_{1}a_{1}t_{1}) \cdot \Delta I_{z}(0)
= \cos(\omega_{CS,i}t_{1}) \left(1 + \frac{a_{1}t_{1}}{a_{0}}\right) \cdot \exp(-R_{2,i}t_{1} - R_{1}a_{1}t_{1}) \cdot \Delta S_{noe}
\operatorname{Im}\{I_{ij}(t_{1})\} = \sin(\omega_{CS}t_{1}) \cdot \sigma_{ij}(a_{0} + a_{1}t_{1}) \cdot \exp(-R_{2,i}t_{1} - R_{1}a_{0} - R_{1}a_{1}t_{1}) \cdot \Delta I_{z}(0)
= \sin(\omega_{CS,i}t_{1}) \left(1 + \frac{a_{1}t_{1}}{a_{0}}\right) \cdot \exp(-R_{2,i}t_{1} - R_{1}a_{1}t_{1}) \cdot \Delta S_{noe}
\Delta S_{noe} = \sigma_{is}a_{0} \cdot \exp(-R_{1}a_{0}) \cdot \Delta I_{z}(0)$$
(14)

In a normal NOESY experiment, the intensity of the NOE cross-peak, ΔS_{noe} , can be evaluated after the first dimension and the fixed mix t_{mix} period.

$$Re\{\Delta S(t_1)\} = \cos(\omega_{CS}t_1) \cdot \exp(-R_2t_1) \cdot \Delta S_{noe}$$

$$Im\{\Delta S(t_1)\} = \sin(\omega_{CS}t_1) \cdot \exp(-R_2t_1) \cdot \Delta S_{noe}$$

$$\Delta S_{noe} = \sinh(\sigma_{is}t_{mix}) \cdot \exp(-R_1t_{mix}) \cdot \Delta I_z(0)$$
(9)

In the srNOESY experiment, the t_{mix} period depends on the t_1 time period.

$$t_{mix} = \sum_{i=0}^{N} a_i t_1^i \tag{10}$$

In the conventional NOESY experiment, only the N=0 term is present. In this study, the srNOESY experiment utilizes mixing times with N=1 (linear) and N=2 (quadratic) time dependencies.

$$t_{mix} = a_0 + a_1 t_1 \tag{11}$$

The srNOESY cross-peak likewise evolves for a two-spin system by combining Eqs. (6) and (8):

In a conventional NOESY, the cross-peak evolves during t_1 and decays exponentially by R_2t_1 . The decay component can be isolated from Eq. (9).

$$D_{\text{NOESY}}(t_1) = \exp(-R_2 t_1) \tag{15}$$

This function gives the cross-peak a Lorentzian shape.

In the srNOESY, the cross-peak decay includes the contribution from the NOE build-up. Its contribution to the shape of the peak and width can also be isolated from Eq. (14).

$$D_{\text{srNOESY}}(t_1) = \left(1 + \frac{a_1 t_1}{a_0}\right) \cdot \exp(-R_{2,i} t_1 - R_1 a_1 t_1)$$
 (16)

The function increases in intensity before a more rapid exponential decay. The resulting spectrum (Fig. 1) has a non-Lorentzian lineshape closer to a Lorentz-to-Gaussian lineshape or the first lobe of an offset sine-bell function. Differences between the srNOESY decay function and apodization functions are described in the Discussion.

The diagonal peaks adopt the following form in the srNOESY experiment, using Eqs. (6) and (8).

$$Re\{\Delta S(t_1)\} = \cos(\omega_{CS}t_1) \cdot \sinh(\sigma_{is}a_0 + \sigma_{is}a_1t_1) \cdot \exp(-R_2t_1 - R_1a_0 - R_1a_1t_1) \cdot \Delta I_z(0)$$

$$Im\{\Delta S(t_1)\} = \sin(\omega_{CS}t_1) \cdot \sinh(\sigma_{is}a_0 + \sigma_{is}a_1t_1) \cdot \exp(-R_2t_1 - R_1a_0 - R_1a_1t_1) \cdot \Delta I_z(0)$$
(12)



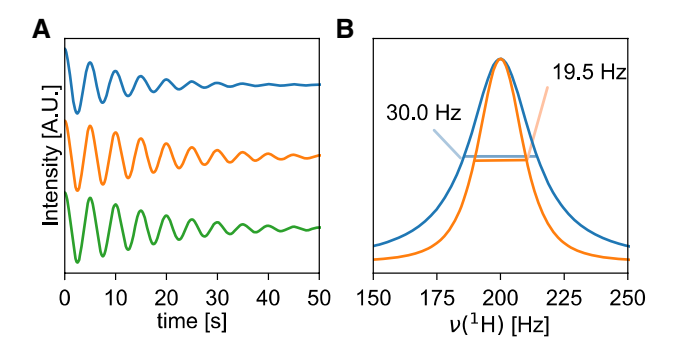


Fig. 1 Simulation of the **a** free induction decays (FIDs) and **b** Fourier transformed spectra for a reference NOESY cross-peak (blue), an srNOESY cross-peak modeled with Eq. (12) and a $\sin (\sigma_{is}t)e^{-\rho t}$ function (orange), and an srNOESY cross-peak modeled with Eq. (14) and a $\sigma_{is}t \cdot e^{-\rho t}$ function (green). The FIDs and spectra were simulated using a 2-spin system with the following parameters for spin 'i': ν =200 Hz, τ_c =4.9 ns, R_2 =30 π s⁻¹, R_1 =1.0 s⁻¹ and a σ_{is} =2.0 s⁻¹ (r_{HH} =2.2 Å). The reference FID was simulated with a 50 ms mixing time, and the srNOESY FIDs were simulated with a_0 =50 ms and a_1 =4. The full-widths at half-height (FWHH) are labeled for each peak in the FT spectra in panel (b). The FT spectra for the two srNOESY cross-peaks (green and orange) are identical at this magnification

Results

The srNOESY-HSQC pulse sequence (Fig. 2) was modified from a conventional ${}^{1}\text{H-NOESY-}{}^{15}\text{N-HSQC}$ (NOESY-HSQC) to include a t_{mix} that increases with the ${}^{1}\text{H}$ evolution period (t_{I}) according to Eq. (11). The conventional (reference) NOESY-HSQC used a constant t_{mix} , and it was collected with the same parameters and t_{mix} =a₀.

Two well-characterized protein systems of very different molecular size were selected to validate this method: ubiquitin (98 amino acids, aa, 10.9 kDa, including a 22 aa N-terminal His₆ tag) and the influenza hemagglutinin fusion peptide domain bound to large, isotropically tumbling bicelles (HAfp-bicelles, 30 aa with 2 H-DMPC/DHPC bicelles at a molar ratio, q, of 0.44). Based on 15 N relaxation experiments (see Fig. S1, Supplementary Information), the τ_c for ubiquitin is 4.25 ± 0.03 ns at 25 °C and the τ_c for HAfp-bicelles is 18.95 ± 0.14 ns at 32 °C. The calculated equivalent globular protein molecular weight for the HAfp-bicelle system is ca. 49.5 kDa, consistent with a 450 aa globular protein (Cavanagh et al. 2007; Nelson and Cox 2013). For the enhanced srNOESY–HSQC of ubiquitin, an a_1 of 4 with a base NOE mix time (a_0) of 50 ms was used, whereas

$$Re\{\Delta S(t_1)\} = \cos(\omega_{CS}t_1) \cdot \cosh(\sigma_{is}a_0 + \sigma_{is}a_1t_1) \cdot \exp(-R_2t_1 - R_1a_0 - R_1a_1t_1) \cdot \Delta I_z(0)$$

$$Im\{\Delta S(t_1)\} = \sin(\omega_{CS}t_1) \cdot \cosh(\sigma_{is}a_0 + \sigma_{is}a_1t_1) \cdot \exp(-R_2t_1 - R_1a_0 - R_1a_1t_1) \cdot \Delta I_z(0)$$
(17)

A Taylor expansion for the $\cosh(\sigma_{is}t)$ function shows that the diagonal decays initially with an exponential function:

$$\Delta I(t) = \exp(-R_1 t) \tag{18}$$

In the srNOESY, the diagonal peak decay includes the additional intensity decay from the NOE transfer:

$$D_{\text{srNOESY}}(t_1) = \exp(-R_{2,i}t_1 - R_1a_1t_1)$$
(19)

Altogether, the srNOESY produces sharper cross-peaks but the diagonal peaks are broader.

an a_1 of 2 and a_0 of 25 ms was employed for HAfp-bicelles. These parameters were found to be optimal (see Fig. S2, S3, Supplementary Information), given the difference in 1 H R $_1$ between the two systems. For example, an a_0 of 100 ms for ubiquitin and 75 ms for HAfp-bicelles only produced modest improvements in resolution (ca. 1–9%) since the crosspeak intensity is nearer to the decay portion of the evolution, rather than the buildup. We also tested quadratic functions for Eq. (10), but we found that linear functions produced the

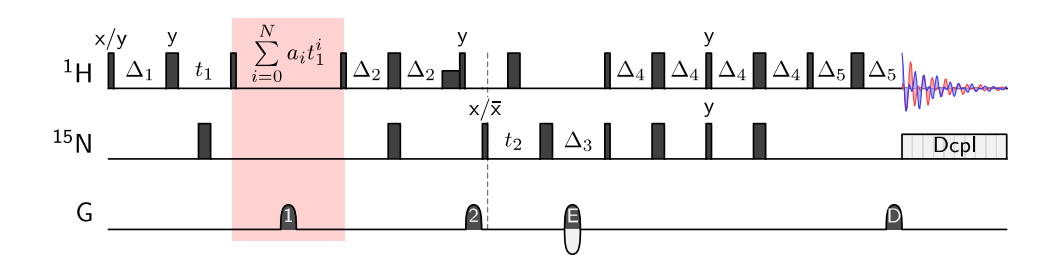


Fig. 2 The srNOESY–HSQC pulse sequence. The pulse sequence is based on the Bruker NOESY–HSQC pulse sequence (noesyhsqcf-3gpsi3d) with the NOE mixing time modified to increment with the t_1 evolution delay in the F_1 dimension. Thin lines represent hard 90° pulses and thick lines represent hard 180° pulses. States-TPPI phase discrimination in F_1 was achieved by incrementing the phase of the $^1\mathrm{H}$ 'x/y' 90° pulse by 90°. Echo-antiecho phase discrimination in F_2

was achieved by incrementing the phase of the 15 N 'x/-x' pulse by 180 ° and inverting the sign of the encoding gradient, labeled 'E'. A WALTZ-16 decoupling scheme was used in collecting the direct dimension FID (F_3) (Shaka et al. 1983). A minimum of eight-steps in the phase cycle were collected. See the pulse program for phase cycle and delay details (Kay et al. 1992; Muhandiram et al. 2007)



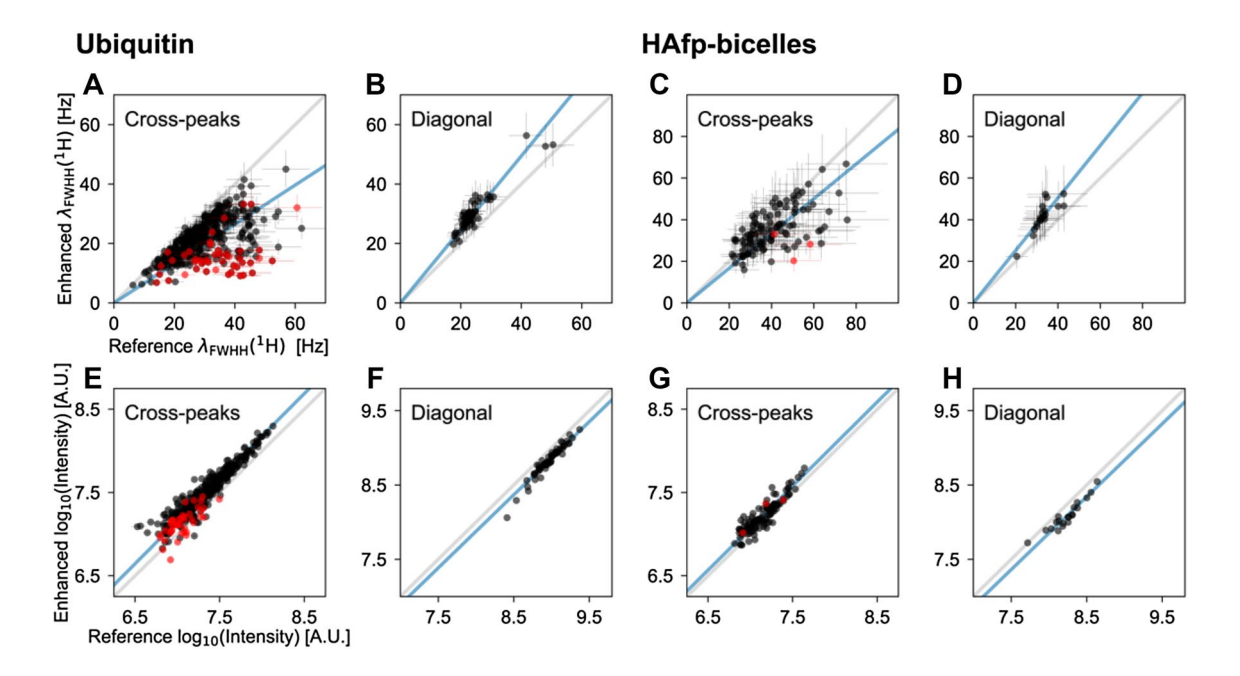


Fig. 3 Comparison plots of the **a-d** 1 H indirect dimension FWHH linewidths and **e-h** log intensity correlations between a reference NOESY-HSQC and an enhanced srNOESY-HSQC. An a_0 of 50 ms and an a_1 of 4 were used in the ubiquitin experiments, while an a_0 of 25 ms and an a_1 of 2 were used in the HAfp-bicelles experiments. Visual guide 1:1 lines are shown in gray, and the linear regression lines (intercept=0) are shown in blue. The red circles represent sin-

gle peaks in the reference experiment that are resolved into two peaks in the enhanced experiments. For these peaks, average values were calculated in the enhanced experiment. The $1-\sigma$ (68.8%) confidence interval of the 1H direct dimensions for these two experiment pairs was calculated and used to estimate the error in (**a-d**), using estimated linewidth fit errors (see Fig. S4, S5, Supplementary Information). The error bars are smaller than the markers in (**e-h**)

best resolution enhancements (see Fig. S3a, Supplementary Information).

In comparison to a conventional (reference) NOESY-HSQC, the srNOESY-HSQC produces average cross-peak linewidth reductions of $31 \pm 1\%$ for ubiquitin and $18 \pm 2\%$ for HAfp-bicelles in the indirect ¹H dimension (Fig. 3a, c). The corresponding resolution enhancement is $45 \pm 2\%$ for ubiquitin and $22 \pm 1\%$ for HAfp-bicelles. A comparison of the linewidths for the ¹⁵N indirect and ¹H direct dimensions (see Fig. S4, Supplementary Information) shows that both experiments have the same resolution in the other dimensions. In contrast, the diagonal peaks receive a reduction in resolution in the indirect ¹H dimension with an average linewidth increase of $24 \pm 2\%$ for ubiquitin and $26 \pm 3\%$ for HAfp-bicelles (Fig. 3b, d). In principle, the broadened diagonal peaks could pose a problem for cross-peaks that are very close to the diagonal, although this was not an issue in resolving any of the ¹H^N-¹H^N cross-peaks in ubiquitin and HAfp-bicelles.

An average increase in signal intensity was also observed for the cross-peaks in the srNOESY-HSQC spectra (Fig. 3e, g). Similar to the resolution enhancements, the opposite effect is observed for the peaks along the diagonal (Fig. 3f, h). The average intensity enhancement is $44 \pm 1\%$ for ubiquitin and $20 \pm 2\%$ for HAfp-bicelles, while the diagonal peaks display an average intensity reduction of

 $26\pm2\%$ for ubiquitin and $29\pm2\%$ for HAfp-bicelles. The srNOESY-HSQC intensities are highly correlated to the reference NOESY-HSQC (R²>0.97). The improved sensitivity of the srNOESY-HSQC revealed many new peaks in comparison to the reference NOESY-HSQC. The reference NOESY-HSQC had 428 cross-peaks for ubiquitin, whereas the srNOESY-HSQC had 635 cross-peaks—a total of 207 (48%) more peaks. The reference NOESY-HSQC for HAfp-bicelles had 119 cross-peaks, while the srNOESY-HSQC had 136 cross-peaks peaks—a total of 17 (14%) more peaks.

Most of the new peaks in the srNOESY-HSQC (162 for ubiquitin and 14 for HAfp-bicelles) can be identified from a conventional NOESY-HSQC with a longer mixing time. The remaining 45 new peaks for ubiquitin and 3 new peaks for HAfp-bicelles were resolved by the enhanced resolution of the srNOESY-HSQC (red points in Fig. 3). The fewer number of new peak assignments is expected for HAfpbicelles because HAfp is a small molecule with nearly all of its resonances already resolved, even though the HAfp complex with bicelles is a significantly larger system. New peaks represent either new assignments, or J_{HH} -couplings in the case of ubiquitin. Visible examples of the resolution enhancements for both cases can be seen in the matched contour plots for each protein (Fig. 4). For ubiquitin, new assignments were found for V5 $H^{\gamma 1}$ and $H^{\gamma 2}$, G10 $H^{\alpha 2}$ and $H^{\alpha 3}$, L15 H^{α} and V17 H^{α} , K27 $H^{\delta 2}$ and $H^{\delta 3}$, and Q41 $H^{\beta 2}$ and



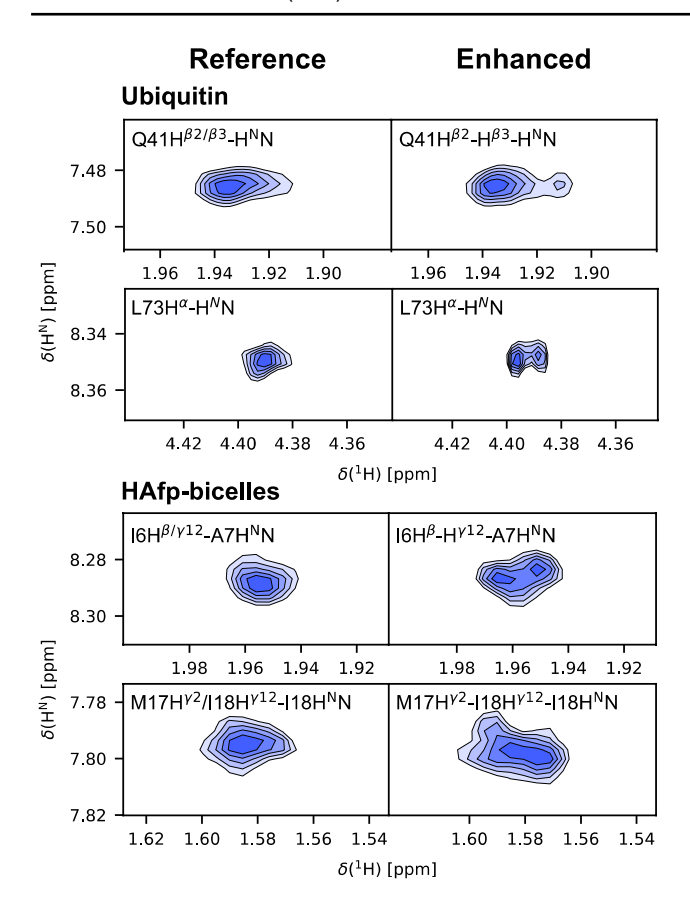


Fig. 4 Selected contour plots of cross-peaks from the reference NOESY–HSQC (left) resolving into two peaks in the enhanced srNOESY–HSQC experiment (right). L73 $\,\mathrm{H}^{\alpha}$ shows a resolved $\,\mathrm{J}_{\mathrm{HH}^{-}}$ coupling whereas other contour plots represent the deconvolution of two discrete spins. Contour plots were prepared by summing the $^{15}\mathrm{N}$ dimension over its FWHH. The lowest contour represents the FWHH. The NOE peaks were identified from literature assignments (Cornilescu et al. 1998; Lorieau et al. 2010)

 $H^{\beta3}$. Resolved peaks in the HAfp-bicelle system include G8 $H^{\alpha2}$ and $H^{\alpha3}$, I6 H^{β} and $H^{\gamma12}$, M17 $H^{\gamma2}$ and I18 $H^{\gamma12}$. Matched contour plots, with accompanying ^{1}H cross sections, for all occurrences of resolved peaks in the srNOESY–HSQC can be found in the SI (see Fig. S6–S9, Supplementary Information). Cross-peaks were assigned from literature chemical shifts and strips from the srNOESY–HSQC spectra (Cornilescu et al. 1998; Lorieau et al. 2010).

The distance restraints were calculated using calibration plots as described in the SI (see Fig. S10, Supplementary Information) and Discussion below. They were plotted to compare their accuracy with the reference experiment (Fig. 5a, b). Interatomic $^1H^{-1}H$ distances from the reference NOESY–HSQC and enhanced srNOESY–HSQC are highly correlated ($R^2 > 0.99$), with linear regression slopes of 1.002 ± 0.003 for ubiquitin and 1.006 ± 0.008 for HAfp-bicelles. The conventional and enhanced experiments yield the same distance restraints.

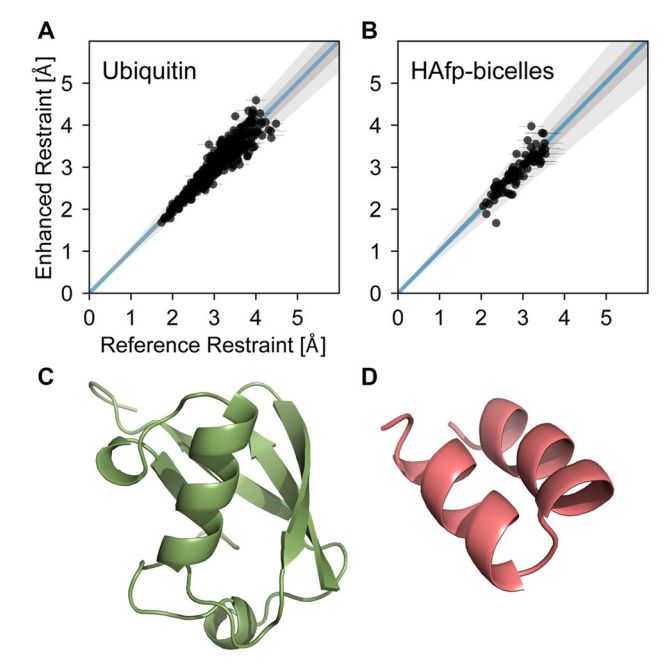


Fig. 5 Comparison of calculated distance restraints for the reference NOESY–HSQC and the enhanced srNOESY–HSQC for a ubiquitin and b HAfp-bicelles. Shaded regions represent the $1-\sigma$ (5.3% and 6.2%, ubiquitin and HAfp, dark gray) and $2-\sigma$ (12.2% and 16.1%, ubiquitin and HAfp, light gray) confidence intervals for the data. Error bars represent the error in the peak intensity propagated through the distance calibration. The solution NMR structures are shown for \boldsymbol{c} ubiquitin and d HAfp generated with the inclusion of restraints from the enhanced srNOESY–HSQC. The original NMR restraints were obtained from the protein data bank (PDB IDs: $1D3Z^{18}$ and $2KXA^{19}$), and matched NOE restraints were replaced with those from the enhanced srNOESY–HSQC in an XPLOR-NIH refinement

We refined the structures of ubiquitin and HAfp with the distance restraints from the srNOESY–HSQC (Fig. 5c, d). The structures are superimposable to the published structures. The backbone heavy-atom root mean square deviations between our refined structures and the previously published structures are 0.24 Å and 0.10 Å for ubiquitin and HAfp, respectively (Cornilescu et al. 1998; Lorieau et al. 2010). The refinement statistics show that structures calculated from srNOESY–HSQC restraints have a comparable accuracy to published values (see Tables S1 and S2, Supplementary Information).

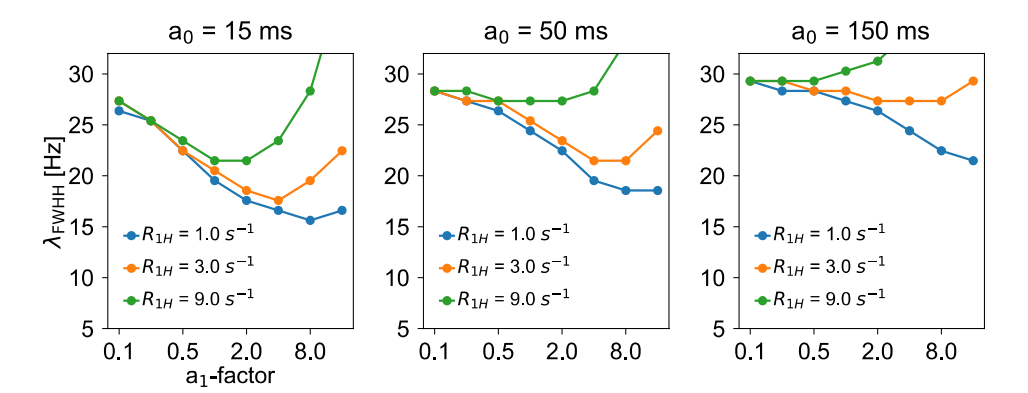
Discussion

Optimal parameters and molecular size

According to Eq. (16), the reduction in peak linewidth and the degree of resolution enhancement depends on the a_0 and a_1 parameters as well as the ¹H R₁ rate of spins (Fig. 6).



Fig. 6 Simulation of the srNOESY cross-peak FWHH as a function of the a_1 -factor, the effective 1H R $_1$ and the NOESY mix time (a_0). The NOE rate was kept fixed at $\sigma_{is} = 2.5 \text{ s}^{-1}$ ($r_{is} = 2.2 \text{ Å}$, $\tau_c = 4.9 \text{ ns}$) and the peaks were simulated with an R $_2$ of 30π s $^{-1}$



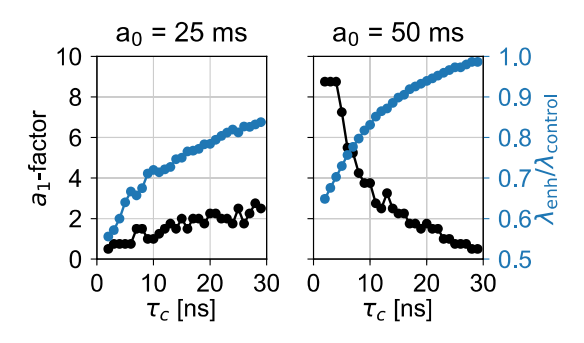


Fig. 7 Simulated optimal a_1 -factors and linewidth reductions at the FWHH as a function of the molecular tumbling time, τ_c . Simulations were conducted for an a_0 of 25 ms and 50 ms, which are optimal for large and mid-size molecules, respectively. Simulations were conducted using Eqs. (4), (5), (9) and (12). The 1 H R_1 was made equal to the modeled NOE, σ_{ij} , and the 1 H R_2 was made equal to 2.5 σ_{ij} π s $^{-1}$

Generally, larger systems have longer tumbling times and larger R_1 rates, and they require shorter a_0 and smaller a_1 parameters to achieve maximum resolution enhancement.

Ideally, a resolution enhancement scheme would improve or remain unchanged as the size of the molecular system increases. Resolution enhancements were observed for the two protein systems in this study, but a less significant improvement was observed for the larger HAfp-bicelle system. The resolution enhancements are smaller for larger systems because the degree of enhancement does not depend on the tumbling time, whereas the linewidths of cross-peaks are directly proportional to the tumbling time. For this reason, the degree of enhancement is reduced for larger systems where it would be most useful. In our case, the reduction in average linewidth is reduced from $31 \pm 1\%$ for ubiquitin to $18 \pm 2\%$ for HAfp-bicelles. This reduction in resolution enhancement can be attributed to the increase in the R_1 rate, which also increases proportionally with the size of the molecular system.

The simulations in Fig. 7 shows the optimal a_0 and a_1 parameters for different rotational tumbling times, τ_c . For the best resolutions, the a_0 parameter should be as short as possible. However, shorter a_0 values also reduce the intensity of

cross-peaks. Nevertheless, shorter a_0 values in the srNOESY experiment can be used in comparison to the t_{mix} times in a conventional NOESY because cross-peaks have greater intensity in the srNOESY experiment.

In selecting optimal a_0 and a_1 parameters, we suggest using an a_0 value that is short enough to give good crosspeak intensity (5–20% of the diagonal intensity) and still in the NOE linear build-up regime, then selecting the optimal a_1 parameter for a given τ_c with Fig. 7 as a guide. The selection of an a_0 parameter that is too long and near the NOE intensity maximum will produce cross-peaks with linewidths that are larger than the conventional NOESY experiment, according to Eq. (16).

For molecules with tumbling times up to 10 ns (ca. 24 kDa), an a_0 of 50 ms can be used with an a_1 parameter selected from Fig. 7. For molecules with tumbling times of 10–20 ns (up to ca. 58 kDa), an a_0 of 25 ms will produce greater resolution enhancements. Shorter a_0 values are more complementary to larger molecular systems because the NOE transfer is much more efficient for larger τ_c values (Eq. (4)).

The reduced resolution enhancement for larger systems could also be circumvented, in part, with partial deuteration. Partial deuteration decreases the density of $^1\mathrm{H}$ spins, thereby reducing the linewidths of $^1\mathrm{H}$ peaks as well as spin diffusion pathways (LeMaster 1989). The principal drawback to partial deuteration is a reduction in $^1\mathrm{H}$ signal intensity. However, the lower abundance of $^1\mathrm{H}$ spins is partially compensated by the increase in intensity from sharper peaks (Kalbitzer et al. 1985). The srNOESY experiments would achieve an additional resolution enhancement through a reduction in the $^1\mathrm{H}$ R $_1$ rate. A smaller $^1\mathrm{H}$ R $_1$ rate would enable larger a_0 and a_1 parameters and greater resolution enhancements.

Information content of the srNOESY lineshape

The srNOESY cross-peak does not contain more information than the NOESY cross-peak at maximum intensity. Figure 8a shows the predicted cross-peak buildup using Eq. (6). A short mixing time (t_{short}, blue dashed lines) is typically



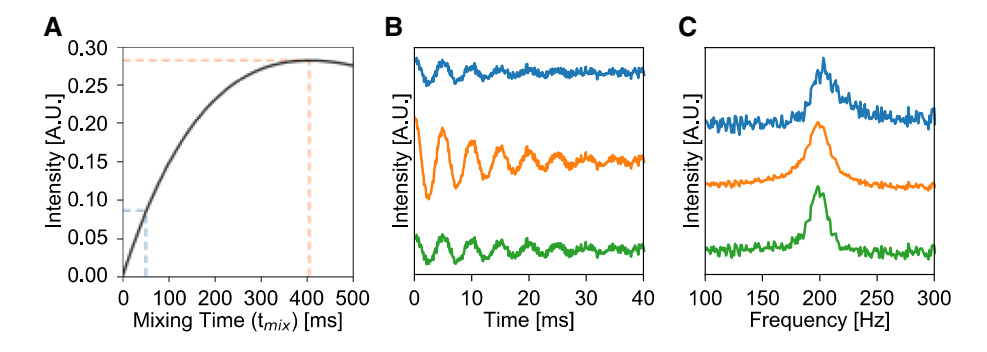


Fig. 8 Comparison of the simulated intensities and FIDs for NOESY cross-peaks at a short mixing time (blue), a cross-peak at a mixing time with maximum intensity (orange) and a srNOESY cross-peak (green). **a** Simulation of the cross-peak build-up as a function of the NOE mixing time for a cross-peak between two 1 H spins with an NOE rate (σ_{ij}) of 1.9 s⁻¹ and the 1 H R₁ of 2.5 s⁻¹. The NOE build-up was modeled with Eq. (6). **b** The simulated FIDs in the t_{1} dimension

for the cross-peak at a short mixing time (blue, $t_{short} = 50$ ms), the cross-peak with maximum intensity (orange, $t_{max} = 406$ ms) and the srNOESY crosspeak (green, $a_0 = 50$ ms and $a_1 = 4$). A random Gaussian noise equal to 10% of the initial FID t_{max} intensity $(1-\sigma)$ was added to each FID. The FIDs were simulated with an R_2 of 25π s⁻¹. c The corresponding Fourier transformed spectra of the simulated FIDs without apodization

selected in a conventional NOESY since the cross-peak intensity more accurately encodes the distance between two $^1\mathrm{H}$ spins (Neuhaus and Williamson 2000). At longer mixing times, the NOE cross-peak reaches a maximum intensity (t_{max} , orange dashed lines), and the peak intensity encodes the R_1 of the spin. The corresponding FIDs (Fig. 8b) in t_1 are shown in panel B. Without noise, the information content of the FID at t_{short} (blue) and the FID at t_{max} (orange) would be the same. However, both FIDs are subject to experimental noise, and consequently, the FID at t_{max} contains more lineshape information. This can be seen in the larger amplitude oscillations later in the FID.

Likewise, the corresponding srNOESY cross-peak (green) encodes the distance between spins in its intensity, yet it also contains much of the resolution information from the FID at t_{max} , with the larger amplitude oscillations later in the FID. The srNOESY cross-peak contains more lineshape information than the FID at t_{short} , yet it still contains less information than the FID with t_{max} .

Comparison to apodization

Apodization is the process of scaling an FID signal with a function to emphasize different regions of the time-domain data. The scaling function is convolved in the Fourier transformed spectrum to change peak shapes and emphasize either the signal-to-noise or the sharpness of peaks. Apodization functions generally fall under two classes: signal enhancing, using functions like an exponential decay or a Gaussian function, and "resolution enhancing," using Lorentz-to-Gauss window functions or the first lobe of an offset sine-bell function. The former sacrifices peak widths for an increased signal-to-noise ratio whereas the latter sacrifices signal-to-noise to improve peak linewidths. In either case,

apodization only impacts the appearance of the Fourier Transformed spectrum.

As long as noise is non-deterministic in an existing dataset, mathematical operations, including apodization, cannot introduce new information in the dataset. "Resolution enhancing" apodization is a misnomer since the resolution of peaks, to potentially introduce new peaks, is not achieved. A more accurate term would be "peak sharpening" apodization. An experimental procedure only enhances the resolution if it can resolve new features in the dataset. For example, a mathematical procedure that replaces peaks with delta-functions may appear to have infinite resolution, yet no new peaks are resolved by this process.

Conceptually, the resolution enhancement of the srNOESY experiment may appear analogous to peak sharperning apodization. However, the srNOESY experiment will contain more lineshape information than the conventional NOESY experiment if both are collected in the linear, short mixing time regime. To get analogous spectral information from a conventional NOESY, the NOESY must be collected near the cross-peak intensity maximum with an aggressive peak sharpening apodization scheme. The drawback of this approach is that the cross-peak intensity does not accurately encode the distances between ¹H spins.

Figure 9 demonstrates contour plots for the cross-peak lineshapes of ubiquitin using the conventional NOESY and the srNOESY with a short mixing time (t_{mix} and a_0 of 50 ms) and a conventional NOESY collected with longer t_{mix} that is closer to the NOE maximum (t_{mix} of 250 ms). The conventional NOESY with a longer mixing time and aggressive apodization was able to resolve 18 of the 45 newly resolved peaks from the srNOESY experiment (see Fig. S6, Supplementary Information).

For D21H $^{\beta2}$, the peak appears broadened in the conventional NOESY with a short t_{mix} . The srNOESY resolves the



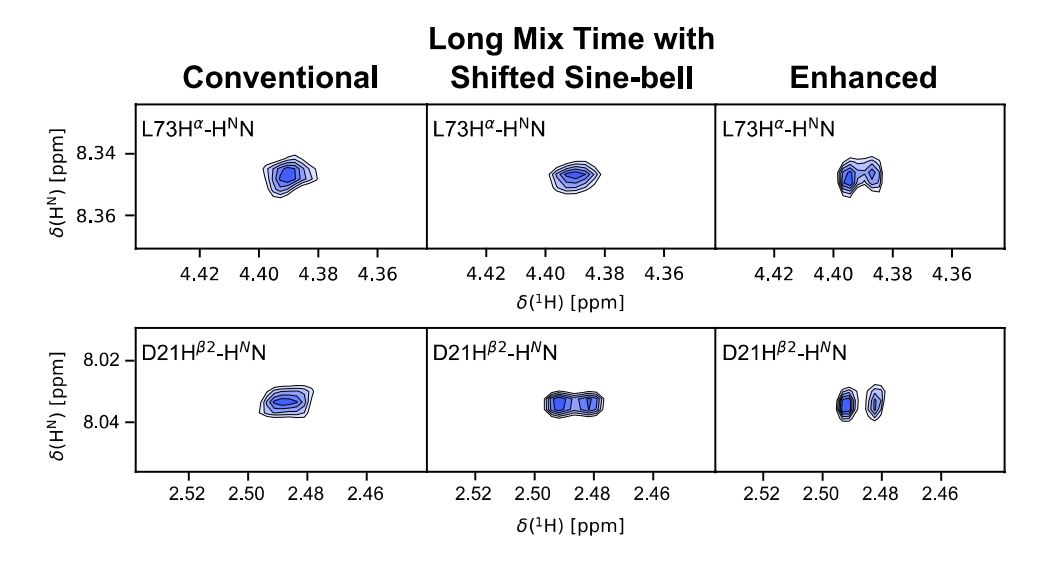


Fig. 9 Contour plots from a conventional NOESY–HSQC (t_{mix} =50 ms), a conventional NOESY–HSQC with a long mixing time (t_{mix} =250 ms) and a peak sharpening shifted sine-bell window apodization function, and a srNOESY–HSQC (a_0 =50 ms, a_1 =4). Contour plots are presented from the ubiquitin datasets with otherwise matched experimental conditions. From left to right for L73 H $^{\alpha}$, the FWHH of the peaks are 27.3, 24.1, 12.6 and 10.3 Hz. From left to right for D21 H $^{\beta 2}$, the FWHH of the peaks are 30.1, 20.8, 13.6, 19.9

and 11.2 Hz. The conventional NOESY–HSQC with short mixing time and the srNOESY–HSQC were processed with a first-order sine-bell window with initial value of 0.45π and a final value of 0.90π . The NOESY–HSQC with a long mixing time was apodized using a first-order sine-bell window with initial value of 0.375π and a final value of 1.0π . All apodization functions were applied using the NMRPipe software package (Delaglio et al. 1995)

splitting of the two peaks, which is also recovered in the conventional NOESY with a long mixing time and aggressive peak sharpening apodization. By contrast, L73H $^{\alpha}$ remains a singlet in both conventional NOESY experiments while the srNOESY is able to resolve two peaks for this assignment. This is likely due to a reduced $R_{1,H}$ for this spin, as it is in the dynamic C-terminal tail of ubiquitin. In this case, the $t_{\rm mix}$ would have to be increased substantially from 250 ms to resolve the doublet in the conventional NOESY. However, increasing the $t_{\rm mix}$ could decrease the intensity of other cross-peaks, and it would further reduce the accuracy of the NOEs. Different peaks will also have different $R_{1,H}$ rates, and they will experience maxima at different $t_{\rm mix}$ values. Consequently, a single $t_{\rm mix}$ may not be used to achieve the best resolution of all peaks in a conventional NOESY.

Lineshape and the effect of spin diffusion

Spin diffusion adversely impacts the accuracy of NOE distances, and it is manifested at longer NOE mixing times. We characterized the extent of spin diffusion in our data by plotting the relationship between the cross-peak intensity and the internuclear distance (see Fig. S10, Supplementary Information) from reference structures (Cornilescu et al. 1998; Lorieau et al. 2010).

$$\log(\Delta S) = -m\log r_{ij} + C \tag{20}$$

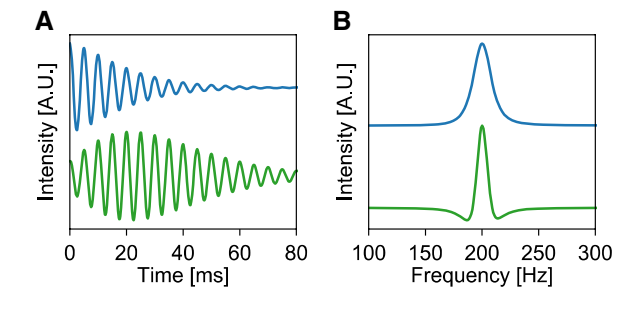


Fig. 10 Comparison of the simulated **a** srNOESY crosspeak FID and **b** corresponding FT spectra for srNOESY cross-peaks with a linear NOE buildup (blue) and a cubic (green) NOE buildup

In the absence of spin diffusion, the slope of the plot, m, should have a value of -6, following Eq. (2). Spin diffusion and relaxation increase the value of this slope. For crosspeaks with high intensity and short r_{ij} distances, the contribution from the direct 2-spin transfer tends to dominate the cross-peak intensity. For more distant spins, the crosspeak intensity is much smaller, and spin diffusion pathways contribute more intensity to the cross-peak relative to the direct 2-spin transfer. Consequently, distant spins appear to have shorter internuclear distances and the experimental slope in Eq. (20) is more positive than -6. With ubiquitin as an example, we calculated a slope 'm' of -3.6 ± 0.1 from the conventional NOESY–HSQC and a slope of -3.4 ± 0.1 from the srNOESY–HSQC. The more positive



slope of the srNOESY–HSQC indicates that the internuclear distances are subject to spin diffusion contamination to a slightly greater extent. This effect is unsurprising because the srNOESY–HSQC increases the mixing time throughout the experiment. The contribution of spin diffusion can be corrected using this procedure.

Additionally, the impact of spin diffusion was not directly observed in the peak line-shapes from the srNOESY–HSQC. In theory, cases with strong spin diffusion pathways may appear distorted if a short a_0 parameter is selected. A simulated example is presented in Fig. 10. The blue FID and FT spectrum represents the srNOESY cross-peak for a linear NOESY buildup, characteristic of a 2-spin transfer, and the green FID and FT spectrum represents a cubic NOESY buildup, characteristic of spin diffusion. The spin-diffusion FID increases significantly in intensity before its decay, producing a lineshape with a distorted baseline. Peaks near this distorted peak will have a diminished intensity.

The srNOESY–HSQC peaks do not appear to have this distortion (see Fig. S8, S9, Supplementary Information). Though we did not observe these distortions in our spectra, their appearance would be avoided by increasing the a_0 parameter in the experiment.

Conclusions

We have shown that a simple modification to the NOESY pulse sequence can improve the resolution of spectra while maintaining the accuracy of distances from a conventional NOESY experiment. Resonances are resolved with reduced linewidths, and new peaks can be identified. The resulting spectra are greatly enhanced, without the use of costly isotopic labeling schemes. The enhancement is more modest for larger systems, yet the srNOESY experiment still presents a useful increase in resolution for both small and large systems to resolve new peaks. The srNOESY pulse program is simple to implement, effective for fully protonated molecules, and readily applied with current technology.

Acknowledgements This work was supported by the National Science Foundation under Grant No. 1651598 and funds from the Department of Chemistry at the University of Illinois at Chicago. This study made use of NMRbox: National Center for Biomolecular NMR Data Processing and Analysis, a Biomedical Technology Research Resource (BTRR), which is supported by NIH Grant P41GM111135 (NIGMS).

References

- Baleja JD, Moult J, Sykes BD (1990) Distance measurement and structure refinement with NOE data. J Magn Reson 87:375–384
- Battiste JL, Wagner G (2000) Utilization of site-directed spin labeling and high-resolution heteronuclear nuclear magnetic resonance for

- global fold determination of large proteins with limited nuclear overhauser effect data. Biochemistry 39:5355–5365
- Borgias BA, Gochin M, Kerwood DJ, James TL (1990) Relaxation matrix analysis of 2D NMR data. Prog Nucl Magn Reson Spectrosc 22:83–100
- Cavanagh J, Fairbrother W, Palmer III, Rance M, Skelton N (2007) Protein NMR principles and practice. Academic Press, Cambridge. https://doi.org/10.1093/cid/cis040
- Chi CN, Strotz D, Riek R, Vögeli B (2018) NOE-derived methyl distances from a 360 kDa PROTEASOME Complex. Chemistry 24:2270–2276
- Cole R, Loria JP, FAST-Modelfree (2003) A program for rapid automated analysis of solution NMR spin-relaxation data. J Biomol NMR 26:203–213
- Cornilescu G, Marquardt JL, Ottiger M, Bax A (1998) Validation of protein structure from anisotropic carbonyl chemical shifts in a dilute liquid crystalline phase. J Am Chem Soc 120:6836–6837
- Delaglio F et al (1995) NMRPipe: a multidimensional spectral processing system based on UNIX pipes. J Biomol NMR 6:277–293
- Dobson C, Olejniczak E, Poulsen F, Ratcliffe R (1982) Time development of proton nuclear overhauser effects in proteins. J Magn Reson 48:97–110
- Ellman JA, Volkman BF, Mendel D, Schulz PG, Wemmer DE (1992) Site-specific isotopic labeling of proteins for NMR studies. J Am Chem Soc 114:7959–7961
- Farrow NA et al (1994) Backbone dynamics of a free and a phosphopeptide-complexed Src homology 2 domain studied by15N NMR relaxation. Biochemistry 33:5984–6003
- Goddard TD, Kneller DG (2008) SPARKY 3. University of California, San Fransisco
- Kalbitzer HR, Leberman R, Wittinghofer A (1985) 1H-NMR spectroscopy on elongation factor Tu from *Escherichia coli*: resolution enhancement by perdeuteration. FEBS Lett 180:40–42
- Kay LE, Keifer P, Saarinen T (1992) Pure absorption gradient enhanced heteronucler single quantum correlation spectroscopy with improved sensitivity. J Am Chem Soc 114:10663–10665
- Lee W, Tonelli M, Markley JL (2015) NMRFAM-SPARKY: enhanced software for biomolecular NMR spectroscopy. Bioinformatics 31:1325–1327
- LeMaster DM (1989) Deuteration in protein proton magnetic resonance. Methods Enzymol 177:23–43
- LeMaster DM, Richards FM (1988) NMR sequential assignment of Escherichia coli thioredoxin utilizing random fractional deuteriation. Biochemistry 27:142–150
- Lipari G, Szabo A (1982a) Model-free approach to the interpretation of nuclear magnetic resonance relaxation in macromolecules. 2. Analysis of experimental results. J Am Chem Soc 104:4559–4570
- Lipari G, Szabo A (1982b) Model-free approach to the interpretation of nuclear magnetic resonance relaxation in macromolecules. 1. Theory and range of validity. J Am Chem Soc 104:4546–4559
- Lorieau JL, Louis JM, Bax A The complete influenza hemagglutinin fusion domain adopts a tight helical hairpin arrangement at the lipid:water interface. Proc Natl Acad Sci 107:11341–11346 (2010)
- Maciejewski MW et al (2017) NMRbox: a resource for biomolecular NMR computation. Biophys J 112:1529–1534
- Macura S, Wüthrich K, Ernst RR (1982a) The relevance of J crosspeaks in two-dimensional NOE experiments of macromolecules. J Magn Reson 47:351–357
- Macura S, Wuthrich K, Ernst RR (1982b) Separation and suppression of coherent transfer effects in two-dimensional NOE and chemical exchange spectroscopy. J Magn Reson 46:269–282
- Marley J, Lu M, Bracken C (2001) A method for efficient isotopic labeling of recombinant proteins. J Biomol NMR 20:71–75
- Muhandiram R, Kay LE (2007) Three-Dimensional HMQC-NOESY, NOESY-HMQC, and NOESY-HSQC. Encycl Magn Reson. https://doi.org/10.1002/9780470034590.emrstm0563



- Nelson DL, Cox MM (2013) Lehninger principles of biochemistry. W. H. Freeman and Company, New York
- Neuhaus D, Williamson MP (2000) The nuclear overhauser effect in structural and conformational analysis. Wiley, New Jersey. https://doi.org/10.1016/0022-2364(92)90256-7
- Ollerenshaw JE, Tugarinov V, Kay LE, Methyl TROSY (2003) Explanation and experimental verification. Magn Reson Chem 41:843–852
- Otten R, Chu B, Krewulak KD, Vogel HJ, Mulder FAA (2010) Comprehensive and cost-effective NMR spectroscopy of methyl groups in large proteins. J Am Chem Soc 132:2952–2960
- Pervushin K, Riek R, Wider G, Wuthrich K (1997) Attenuated T2 relaxation by mutual cancellation of dipole-dipole coupling and chemical shift anisotropy indicates an avenue to NMR structures of very large biological macromolecules in solution. Proc Natl Acad Sci 94:12366–12371
- Rieping W, Bardiaux B, Bernard A, Malliavin TE, Nilges M (2007) ARIA2: automated NOE assignment and data integration in NMR structure calculation. Bioinformatics 23:381–382
- Schimmel PR, Cantor CR (1980) Biophysical chemistry, part II: techniques for the study of biological structure and function. W.H. Freeman, San Francisco
- Schwieters CD, Kuszewski JJ Clore GM (2006) Using Xplor-NIH for NMR molecular structure determination. Prog Nucl Magn Reson Spectrosc 48:47–62

- Shaka AJ, Keeler J, Frenkiel T, Freeman R (1983) An improved sequence for broadband decoupling: WALTZ-16. J Magn Reson 52:335–338
- Smrt ST, Draney AW, Lorieau JL (2015) The influenza hemagglutinin fusion domain is an amphipathic helical hairpin that functions by inducing membrane curvature. J Biol Chem 290:228–238
- Tugarinov V, Kay LE (2005) Methyl groups as probes of structure and dynamics in NMR studies of high-molecular-weight proteins. ChemBioChem 6:1567–1577
- Vögeli B et al (2009) Exact distances and internal dynamics of perdeuterated ubiquitin from NOE buildups. J Am Chem Soc 131:17215–17225
- Vögeli B, Friedmann M, Leitz D, Sobol A, Riek R (2010) Quantitative determination of NOE rates in perdeuterated and protonated proteins: Practical and theoretical aspects. J Magn Reson 204:290–302
- Vuister GW, Bax A (1992) Resolution enhancement and spectral editing of uniformly 13C-enriched proteins by homonuclear broadband 13C decoupling. J Magn Reson 98:428–435
- Weigelt J (1998) Single scan, sensitivity- and gradient-enhanced TROSY for multidimensional NMR experiments. J Am Chem Soc 120:10778–10779

Publisher's Note Springer Nature remains neutral with regard to jurisdictional claims in published maps and institutional affiliations.

